MODELLING FIBRE FANNING IN DIFFUSION-WEIGHTED MRI

Stamatios N. Sotiropoulos, Timothy E. Behrens and Saad Jbabdi

FMRIB Centre, University of Oxford, UK

ABSTRACT

Even if a number of methods have been proposed for resolving crossing fibres from diffusion-weighted (DW) MRI, other complex fibre geometries have drawn minimal attention. In this study, we focus on fibre orientation dispersion induced by within-voxel fanning. We use a multi-compartment, model-based approach to estimate fibre dispersion. A Bingham distribution is employed to represent a continuum of fibre orientations, centred around a main orientation. We evaluate the accuracy of the model for different simulated fanning geometries, under different acquisition protocols and we illustrate the high SNR and angular resolution needs. We apply the proposed model on high-quality, post-mortem macaque data and present whole-brain maps of fibre dispersion.

***Index Terms*—** Deconvolution, Bingham, Dispersion, Macaque

1. INTRODUCTION

It has been almost a decade since the first attempts to resolve complex fibre architectures from diffusion-weighted magnetic resonance imaging (DW-MRI) [1]. Both parametric and non-parametric approaches have been introduced, where characterisation of fibre crossing has drawn much more attention than other patterns (see [2] for a review). Indeed, most of the methods developed so far have been used for detecting discrete sets of fibre orientations. For the majority of parametric cases, these orientations are explicitly included in the model and estimated from the data [3]. In the case of model-free approaches, they are estimated as the local maxima of the diffusion or fibre orientation distribution functions (dODFs/fODFs) [4, 5].

Incorporating information on (discrete) crossing fibres has significantly improved tractography reconstructions. Algorithms that allow for more than a single fibre orientation per voxel are more sensitive to detecting secondary white matter bundles that cross larger ones [6]. However, other complex patterns of intra-voxel axonal organisation still pose challenges to modern tractography [6]. For example, many white matter fibre bundles appear to have a fanning geometry (e.g. corona radiata). At the voxel-level, these fanning geometries indicate that axons do not follow a discrete set of orientations, but a continuum, potentially centred on a mean orientation.

Some of the model-free approaches attempt at reconstructing a continuous ODF, potentially capturing fanning geometries [5]. Seunarine et al have pointed out that these functions may exhibit stretched peaks in the presence of anisotropic fanning or bending [7]. However, the shape of the peaks is not necessarily an accurate description of the precise fanning of underlying axonal fibres. Ad-hoc sharpening and/or regularization of the ODFs are commonly employed [4, 5]; these may not affect the location of the peak orientations, but affect the shape of the function.

We acknowledge funding from the EU CONNECT project (238292), the Wellcome Trust (WT088312AIA), the UK Medical Research Council (G0800578) and the NIH Human Connectome Project (1U54MH091657-01).

A very limited number of model-based approaches have focused on fanning patterns. A model-based deconvolution of the signal using Bingham and Watson distributions is described in [8]. Fanning is explicitly modelled, but the study focused on the reduction in propagated uncertainty with this approach, when tracking using the main orientation of the fanning compartment.

Here, we take a model-based approach to the problem. We explicitly model the effect of fibre fanning on the diffusion signal using a parametric spherical distribution. We are extending the ball & stick model [3] and use an anisotropic Bingham distribution to perform a deconvolution of the signal. Our model is a special case of the one introduced by [8], however by choosing a "stick" single-fibre response kernel, we are achieving an identifiable model. For the first time, we explore the extra information that can be inferred from such a model on the extent, anisotropy and orientation of a fanning compartment, using Monte-Carlo simulations. We also illustrate the potential of such an approach by applying it to high quality post-mortem macaque data.

2. METHODS

2.1. The ball and racket model

The ball and stick model [3] decomposes the signal into a fully isotropic and a perfectly anisotropic compartment:

$$S_k = S_0 \left[(1-f)\exp(-b_k d) + f\exp(-b_k d(\mathbf{g}_k^T\mathbf{v})^2)\right] \quad (1)$$

with $S_k,\ k = 1:M$ the DW signal measured after the application of a diffusion-sensitising gradient with direction $\mathbf{g}_k$ and b value b_k, S_0 the signal without any diffusion weighting, d the mean diffusivity and $f \in [0,1]$ the volume fraction of the anisotropic compartment with orientation $\mathbf{v} = [\sin\theta\cos\phi \quad \sin\theta\sin\phi \quad \cos\theta]^T$, $\theta \in [0,\pi]$ and $\phi \in [0,2\pi)$. If instead of a single fibre orientation $\mathbf{v}$, a continuous distribution of orientations $H(\theta,\phi)$ is assumed for the population [3], the model can be generalized to:

$$\begin{aligned} S_k =& S_0[(1-f)\exp(-b_k d)+ \\ & f\int_0^{2\pi}\int_0^{\pi} H(\theta,\phi)\exp(-b_k d(\mathbf{g}_k^T\mathbf{v})^2)\sin\theta d\theta d\phi] \end{aligned} \quad (2)$$

The above model is a spherical convolution of function H with the single-fibre response kernel $\exp(-b_k d(\mathbf{g}_k^T\mathbf{v})^2)$. The ball and stick model is a special case where H is a delta function, i.e. all axons in a population are assumed parallel to $\mathbf{v}$.

Let $H(\mathbf{v}) = \mathcal{F}_{\mathcal{B}}(\mathbf{v};\mathbf{B})$ be a Bingham distribution of $\mathbf{v}$ with parameter the 3x3 symmetric matrix $\mathbf{B}$, as in [8]. This distribution is axially symmetric, i.e. $\mathcal{F}_{\mathcal{B}}(\mathbf{v};\mathbf{B}) = \mathcal{F}_{\mathcal{B}}(-\mathbf{v};\mathbf{B})$ and its probability density is given by $\mathcal{F}_{\mathcal{B}}(\mathbf{v};\mathbf{B}) = \exp(\mathbf{v}^T\mathbf{B}\mathbf{v})/c_B$, with $c_B =$

$4\pi\ {}_1F_1(1/2;3/2;\mathbf{B})$ and ${}_1F_1(\alpha;\beta;\mathbf{Z})$ the confluent hypergeometric function of the first kind with a matrix argument [9]. Then, substituting into Equation (2), gives the ball and racket model:

$$\frac{S_k}{S_0} = (1-f)\exp(-b_k d) + f\frac{{}_1F_1(1/2;3/2;\mathbf{B} - b_k d\mathbf{g}_k\mathbf{g}_k^T)}{{}_1F_1(1/2;3/2;\mathbf{B})} \quad (3)$$

The Bingham matrix $\mathbf{B}$ is represented as $\mathbf{B} = \mathbf{R}^T\mathbf{B}_{diag}\mathbf{R}$, with $\mathbf{R}$ a rotation matrix and $\mathbf{B}_{diag}$ a diagonal matrix with two non-zero fanning eigenvalues $k_1 \geq k_2 > 0$. The larger the eigenvalues, the less dispersion is modelled. Anisotropic ($k_1 > k_2$) and isotropic ($k_1 = k_2$) fanning can be represented, as Bingham is an assymetric distribution.[1] In the absence of any dispersion, $k_1, k_2 \to \infty$ and the model-predicted signal converges to the one predicted by the ball and stick model. The rotation matrix R is fully described by the three rotation angles θ, ϕ and ψ. These give the mode (main fibre orientation) of the distribution, as well as the orientation along which the biggest fanning extent occurs, in case of anisotropic fanning (main fanning orientation).

The Bingham distribution has been employed to represent a fanning geometry, where a continuum of fibre orientations spread around a main orientation. However, a similar pattern of orientation dispersion can be anticipated for a bending geometry [10]. Therefore, the ball and racket model cannot differentiate between (within-voxel) fanning and bending patterns.

2.2. *Implementation*

A non-linear optimization routine was used to obtain estimates for the model parameters by minimizing the sum of squared residuals. A Levenberg-Marquardt algorithm with a numerical derivation of the Jacobian and a Gauss-Newton approximation of the Hessian was utilised. To preserve the inequality $k_1 \geq k_2$ during optimization, k_2 was transformed so that the ratio $w = k_1/k_2 \geq 1$ was included instead into the model. Other tranformations that ensured valid ranges for the model parameters, included $d \to \lambda^2$, to preserve $d \geq 0$, and $\alpha \to LL + UL * sin^2(\beta)$, to preserve $LL \leq \alpha \leq UL$, where $\alpha = [f,\ k_1,\ w]$. The chosen ranges were $f \in [0,1]$, $k_1 \in [4, 10000]$ and $w \in [1, 100]$. A lower limit was chosen for k_1 to avoid too spherical dispersions and identifiability issues with the ball compartment.

A challenging issue is to provide good starting points for the unknown parameters, in order to avoid the algorithm getting trapped in local minima. Information from the simpler ball and stick model can be used for this purpose. For a certain dataset, the ball and stick model is fitted and the estimates of d, S_0, f, θ and ϕ are used as starting points for the respective parameters of the ball and racket model. To initialize the fanning angle in case of anisotropic fannings, we use the principal eigenvector of the inverse Hessian of the ball and stick cost function evaluated at its minimum; this predicted well the fanning orientation. For k_1 and w, we used a grid search.

3. RESULTS AND DISCUSSION

3.1. Simulations

Using simulations, we tested the robustness of the model estimates for different fanning geometries and acquisition parameters (SNR, number of diffusion-sensitising directions, b value). The ball and racket model was used to simulate the DW signal ($f = 0.6$, $d = 0.0012$ mm^2/s, $S_0 = 100$) and Rician noise was added (SNR=S_0/σ_{noise}). Representative results for different fanning patterns are shown in Fig. 1. The estimated eigenvalues k_1 and k_2 were converted to the more interpretable "dispersion" angles, along the two axes on the fanning plane; the major fanning orientation and the normal direction to it (called minor, from now onwards). The distribution was considered along these two axes and the angles that contained 95% of the distribution were computed. The plots illustrate that the correct pattern is predicted in general, but a relatively high SNR is required. Three main conclusions can be drawn: a) Small dispersions ($< 10^o$) are difficult to estimate robustly. This is because induced changes in the signal are very small. b) High quality data are needed, particularly high SNR, to infer fanning information. Unlike, crossing fibre methods that are sensitive to the signal extrema, fanning patterns change the signal shape around these extrema. Much larger SNR values are therefore needed to preserve this information in the measurements and allow its inference. c) Isotropic profiles seem more difficult to estimate; due to noise, the estimates tend to be slightly anisotropic (clearly evident for the SNR=30 case).

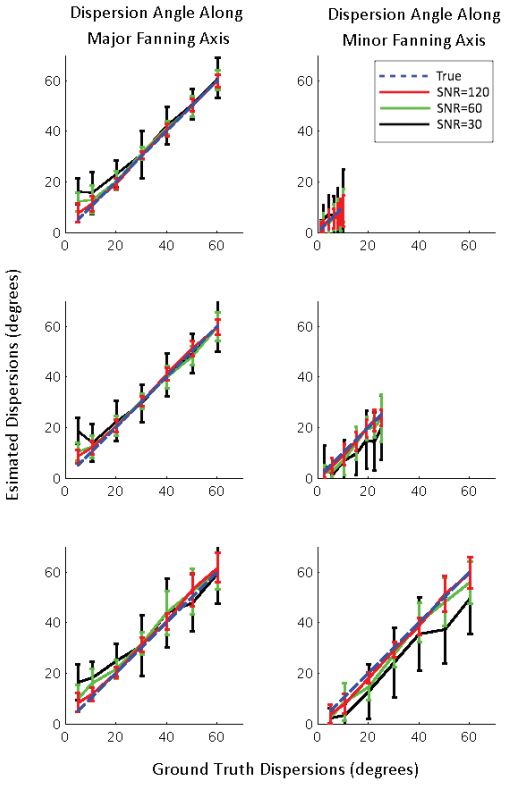


Fig. 1. *Estimated dispersion angles along the major and minor fanning axis, for different fanning patterns. From top to bottom: Very anisotropic patterns, patterns with moderate anisotropy and isotropic patterns. In each case, the fanning extent is varied and the ball and racket estimates are presented for different SNR values (120 shown in red, 60 in green, 30 in black). The errorbars show the mean estimate +/- one standard deviation. across 15 repeats in each case. Other simulation parameters: 120 DW directions, b=2000 s/mm^2.*

Different acquisition scenarios were also simulated (b value=1000,

[1] The model has the same form, when the isotropic Watson distribution is used to parameterize H. Watson is a special case of Bingham with $k_1 = k_2 = \kappa$.

2000, 3000, directions number=60, 120, 240, SNR=15-120) (results not shown). Model estimates improved with higher number of directions and b value, but the need for relatively high SNR persisted. Protocols that are considered adequate for estimating the main fibre orientations (SNR<30, 60 directions, b=1000) seem not high enough for robustly estimating fanning patterns.

The fanning information contained in the ball and racket model was qualitatively compared against the information content in the shape of ODFs, obtained through non-parametric approaches. To make the comparison fair, we simulated the DW signal arising from fanning patterns, using a three-dimensional subvoxel grid, as described in [10], rather than using the model. Briefly, the fanning geometry features were determined by the position of the grid relative to a reference point. The orientation of the anisotropic compartment at each subvoxel was given by the radial line connecting its centre to the reference point. The signal of each subvoxel was then simulated using the ball and stick model [3]. All the signals from the grid were averaged to obtain the simulated DW signal from a fanning pattern. Fanning anisotropy was varied by changing the dimensional anisotropy of the grid. An example of the obtained grids and sets of simulated orientations are shown in Fig. 2. Note that, due to the DW signal symmetry, all methods are sensitive to this set of orientations within a voxel, rather than their exact spatial arrangement.

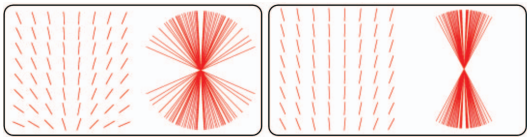


Fig. 2. *Subvoxel grids used to simulate the signal from a fanning pattern. 2D examples are shown. Fibre orientations of each grid, grouped together, are also shown.*

Four representative patterns (very anisotropic, anisotropic, isotropic fanning and no fanning) were used to simulate data. The ball and racket model was fitted to each dataset. ODFs were reconstructed in two different ways: a) An intrinsically sharp dODF was obtained through a constant solid angle (CSA) marginalization of the diffusion scatter pattern [11]. b) The fODF was estimated by a constrained spherical deconvolution of the signal [5]. FSL's ODF estimation toolbox [12] was utilized for the former and the MRtrix package for the latter (J-D Tournier, Brain Research Institute, Melbourne, Australia, http://www.brain.org.au/software/). Both approaches used spherical harmonics of up to 12th order as a basis (lower orders gave broader profiles).

Fig. 3 shows large differences in the potential of the different methods to resolve fanning patterns. In the presence of anisotropic fannings, ODFs tend to have peaks with anisotropic shapes that indicate correctly the fanning orientation. However, the extent and anisotropy of this shape heavily depends on the reconstruction method. The fanning extent is heavily overestimated by the diffusion ODFs. Fibre ODFs are sharper, but also seem to overestimate the fanning extent. The extent of the ball and racket distribution varies significantly, according to the ground truth pattern.

3.2. Post-mortem Macaque Data

We applied the model to high quality post-mortem macaque data, acquired using a 4.7T Brucker scanner, as described in [13]. In short, diffusion weighting was applied along 120 uniformly distributed directions with b=8000 s/mm^2 and voxel size 430x430x430 μm^3.

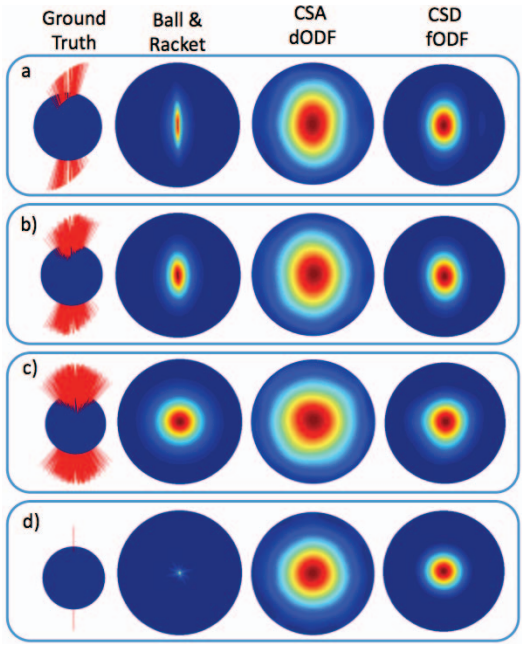


Fig. 3. *Average estimates across 15 simulations of (from left to right): Bingham distributions, Constant solid angle dODFs and Constrained spherical deconvolution fODFs, for four fanning patterns: a) Very anisotropic (1x8x8 grid), b) Anisotropic (4x8x8 grid), c) Isotropic fanning (8x8x8 grid) and d) No fanning. Simulation paremeters were: 120 directions, $b = 2000$ s/mm^2, SNR=60. Spherical harmonics of up to 12^{th} order were used for the ODFs. A Laplace-Beltrami regularization at $\lambda = 0.006$ was used for the dODFs. Colour-code is zero for blue and high for dark red.*

The estimated fanning eigenvalues k_1 and k_2 were converted to dispersion angles, as described in the simulations section. Maps of the mean dispersion extent were generated by plotting on a voxel-by-voxel basis the mean of these two angles, as shown in Figure 4. For better visualization, dispersion values are presented only in white matter, as the values in gray matter and CSF are not particularly meaningful; the anisotropic volume fraction in these regions is small and the fanning parameters degenerate.

Many interesting patterns can be observed in the presented maps. Low fanning indices are generally present in the body of the corpus callosum (CC) (Fig. 4a). A spatial pattern of low-high-low values is observed bilaterally, as we move from medial to lateral callosal regions (single arrow in Fig. 4a). This can be indicative of fibre bending that is expected in the CC body, just before callosal projections enter the centrum semiovale (as pointed out in Methods, the model cannot differentiate between dispersion caused by fanning or bending). Higher dispersion values are predicted in the internal capsule (arrow in Fig. 4b), especially in its posterior limb. An interesting pattern is also observed in the vicinity of most of the cortical gyri. Two representative examples are shown in Fig. 4c, but similar examples can be observed in Fig. 4a and 4b. As white matter approaches the gyral walls, fanning indices gradually increase, having low values midway between two adjacent walls. This pattern suggests coherent bundles that stem/arrive from the gyri and fan in a roughly uniform way towards the gyral walls. Low fanning values along parts of the optic radiation are shown in Fig. 4a (double arrows), where fanning is expected to be minimal.

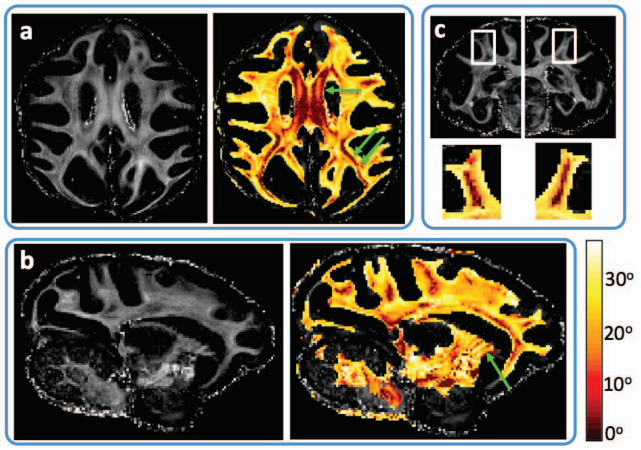


Fig. 4. *Maps of mean fibre dispersion extent in white matter. a) Axial slice of the anisotropic volume fraction f (left) and the dispersion map (right). Dispersion values are shown for white matter only and are superimposed on the f map. b) Sagittal slice of the f and dispersion maps. c) Dispersion values in white matter at the vicinity of cortical gyri. Values in degrees are colour-coded according to the presented legend. Angles are calculated as containing 50% of the distribution, along the major and minor fanning axis.*

Fig. 5a illustrates colour-coded maps of the major fanning orientation, as estimated in each voxel. We can observe spatial continuity in these orientations. An interesting example is in the posterior limb of the internal capsule (shown encircled), where the fanning orientation seems to be anterior-posterior at the posterior regions and changes towards a more medial-lateral orientation at the most anterior regions. The pattern is preserved bilaterally. Fig. 5b and 5c present values for the Bayesian information criterion (BIC) [14], evaluated voxel-wise for the ball and racket model, when a Watson ($k_1 = k_2$) and a Bingham distribution ($k_1 \geq k_2$) are utilized respectively. We can observe that the model with the assymmetric Bingham distribution leads to smaller and more uniform values across the brain (despite having two extra parameters), explaining better the data than the Watson model.

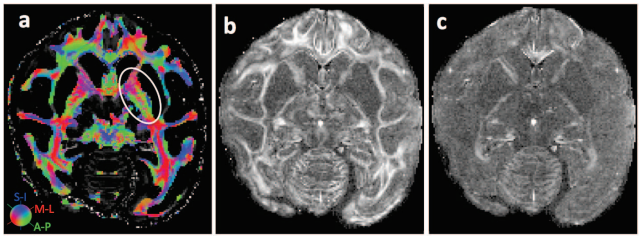


Fig. 5. *a) Major fanning orientation (colour-coded) in white matter. An axial slice is presented. b, c) Bayesian information criterion (BIC) values for the same axial slice, when using in the model a symmetric Watson (b) and an assymetric Bingham distribution (c).*

In summary, we have presented and evaluated a model for directly estimating fibre orientation dispersion, driven by underlying complex geometries, such as within-voxel fibre fanning. The ball and racket is a multi-compartment model that captures both (isotropic) partial volume and an (anisotropic) fibre population. The model assumes that a fibre population can be represented as a continuous distribution of orientations, centred around a main orientation. We illustrated in simulations the high SNR needed to estimate the model parameters robustly and shown its potential in high-quality, post-mortem macaque data. We hope that advances in the MR physics and new acceleration methods for data acquisition that are curently achieved, for instance through the Human Connectome Project (http://humanconnectome.org/), will make the model applicable in-vivo in the very near future.

We should point out that when fitting a single fanning compartment to a region where two fibres cross, the estimated distribution is anisotropic and has an extent that covers both crossing compartments. It is straightforward to extent the model for multiple fanning compartments, however, model selection is necessary to correctly estimate individual fanning patterns and avoid overfitting. We investigate this issue, which will be covered in a future study.

4. REFERENCES

[1] D. S. Tuch, T. G. Reese, M. R. Wiegell, N. Makris, J. W. Belliveau, and V. J. Wedeen, "High angular resolution diffusion imaging reveals intravoxel white matter fiber heterogeneity," *Magnetic Resonance in Medicine*, vol. 48, pp. 577–82, 2002.

[2] K. K. Seunarine and D. C. Alexander, "Multiple fibers: Beyond the diffusion tensor," in *Diffusion MRI: From quantitative measurement to in vivo neuroanatomy*, H. Johansen-Berg and T.E. Behrens, Eds., pp. 55–72. Elsevier, 2009.

[3] T. E. Behrens, M. W. Woolrich, M. Jenkinson, H. Johansen-Berg, R. G. Nunes, S. Clare, P. M. Matthews, J. M. Brady, and S. M. Smith, "Characterization and propagation of uncertainty in diffusion-weighted MR imaging," *Magnetic Resonance in Medicine*, vol. 50, no. 5, pp. 1077–88, 2003.

[4] D. S. Tuch, "Q-ball imaging," *Magnetic Resonance in Medicine*, vol. 52, pp. 1358–72, 2004.

[5] J. D. Tournier, F. Calamante, and A. Connelly, "Robust determination of the fibre orientation distribution in diffusion MRI: non-negativity constrained super-resolved spherical deconvolution," *Neuroimage*, vol. 35, pp. 1459–72, 2007.

[6] S. Jbabdi and H. Johansen-Berg, "Tractography: Where do we go from here?," *Brain Connectivity*, vol. in press, 2011.

[7] K. K. Seunarine, P. A. Cook, M. G. Hall, K. V. Embleton, G. J. M. Parker, and D. C. Alexander, "Exploiting peak anisotropy for tracking through complex structures," in *Proceedings of the IEEE International Conference on Computer Vision Workshop on MMBIA*, 2007.

[8] E. Kaden, T. R. Knosche, and A. Anwander, "Parametric spherical deconvolution: inferring anatomical connectivity using diffusion MR imaging," *Neuroimage*, vol. 37, no. 2, pp. 474–488, 2007.

[9] K. V. Mardia and P. E. Jupp, "Distributions on spheres," in *Directional Statistics*, pp. 159–192. John Wiley & Sons, 2000.

[10] S. Nedjati-Gilani and D. C. Alexander, "Models for fanning and bending sub-voxel structures in diffusion MRI," in *Proceedings of the DMFC MICCAI 2009 Workshop*, London, UK, 2009.

[11] I. Aganj, C. Lenglet, G. Sapiro, E. Yacoub, K. Ugurbil, and N. Harel, "Reconstruction of the orientation distribution function in single and multiple shell q-ball imaging within constant solid angle," *Magnetic Resonance in Medicine*, vol. 64, no. 2, pp. 554–566, 2010.

[12] S. N. Sotiropoulos, I. Aganj, S. Jbabdi, G. Sapiro, C. Lenglet, and T. E. J. Behrens, "Inference on constant solid angle orientation distribution functions from diffusion-weighted mri," Quebec, Canada, June 2011, OHBM Annual Meeting.

[13] H. D'Arceuil, S. Westmoreland, and A. J. de Crespigny, "An approach to high resolution diffusion tensor imaging in fixed primate brain," *NeuroImage*, vol. 35, pp. 553–565, 2007.

[14] G. Schwarz, "Estimating the dimension of a model," *Annals of Statistics*, vol. 6, no. 2, pp. 461–464, 1978.